Energy Advances

ROYAL SOCIETY OF CHEMISTRY

PAPER

View Article Online
View Journal | View Issue

Cite this: *Energy Adv.*, 2025, 4, 424

SnO_2 modified CsH_2PO_4 (CDP) protonic electrolyte for an electrochemical hydrogen pump†

Minal Gupta,[a] Kangkang Zhang[ab] and Kevin Huang *[a]

CsH_2PO_4 (CDP) is a well-known super-protonic conductor. However, it must operate under high humidity conditions to prevent dehydration and fast conductivity decay. Herein, we report that adding hydrophilic SnO_2 into CDP can suppress the rate of dehydration of CDP, thus stabilizing protonic conductivity over a broader range of water partial pressures (p_{H_2O}). A total of seven compositions of $(1 - x)$CDP/$(x)SnO_2$ were prepared, where $5 \leq x \leq 40$ (wt%), and examined for their phasal, microstructural, and vibrational properties using X-ray diffraction, field emission scanning electron microscopy, and Raman spectroscopy. The signature of H_2O retained in SnO_2-added CPD was confirmed by Fourier transform infrared (FTIR) spectroscopy. Among these samples, 18 wt% SnO_2 in CDP stood out, showing a stable protonic conductivity of 0.6×10^{-2} S cm^{-1} at 250 °C, even at 10% H_2O. We also provide data from pre- and post-test characterization to facilitate the understanding of the observed stability improvement and degradation mechanisms. Finally, we show stable H_2 pumping performance of electrochemical cells with pure CDP and 18 wt% SnO_2–CDP electrolyte and Pt/C electrode. Overall, 18 wt% SnO_2–CDP is the best composition, showing stable conductivity under reduced H_2O conditions and 18 wt% SnO_2–CDP electrolyte with Pt/C electrode is the best membrane electrode assembly (MEA) for electrochemical H_2 pumping for lower water partial pressure applications.

Received 6th December 2024,
Accepted 5th January 2025

DOI: 10.1039/d4ya00606b

rsc.li/energy-advances

1. Introduction

Solid acid electrolytes (SAEs) exhibiting high protonic conductivity are of great interest for electrochemical devices such as fuel cells, electrolyzers, and H_2 pumps.[1–4] A representative family of SAEs has a general formula of $M_xH_y(AO_4)_z$, where M = Cs, Na, Rb, NH_4, K, and Li; A = P, S, As, and Se, and x, y, and z are numerals.[5,6] Among these solid acids, CsH_2PO_4 (CDP) containing PO_4 tetrahedra exhibits the highest proton conductivity.[7–9] At 230 °C, CDP transforms from a monoclinic to a cubic phase (also known as the super-protonic phase), triggering gigantic increases in proton conductivity from 10^{-6} S cm^{-1} to 10^{-2} S cm^{-1}.[9] This super-protonic phase is stable up to 250 °C, after which it starts to gradually lose conductivity due to dehydration causing the phase change to less conductive $Cs_2H_2P_2O_7$.[10,11] Maintaining sufficiently high humidity to prevent dehydration is crucial for practical applications of CDP. The higher the operating temperature, the higher humidity is required. Within 230–250 °C, a minimum of 35–38% H_2O (or partial pressure of H_2O, p_{H_2O}) is needed to prevent dehydration of CDP.[12–14] In many practical applications, however, such a high H_2O requirement limits the utility of CDP-based electrochemical devices.

To improve the stability of CDP under lower p_{H_2O}, mixing CDP with oxides or other protonic conductors has been attempted. For example, enhanced stability and conductivity of CDP were reported by adding 10 wt% cerium pyrophosphate (CeP_2O_7).[15] The addition of tin pyrophosphate (SnP_2O_7) to CDP was found to improve the low-temperature conductivity of CDP.[16] Similarly, the SiP_2O_7/CDP composite has also been used as an electrolyte for steam electrolysis,[11] H_2 separation of ammonia,[17] and fuel cells[18] with p_{H_2O} = 0.30–0.47 atm. Apart from metal pyrophosphates (MP_2O_7), neodymium phosphate hydrate ($NdPO_4 \cdot xH_2O$) as a dopant was also found to improve both conductivity and stability of CDP by thermally stable hydrate water in $NdPO_4 \cdot xH_2O$.[7]

On the other hand, adding simple metal oxides into CDP has also been studied, but with conflicting results. For example, TiO_2 and SiO_2 have been found to stabilize CDP in sealed containers,[12,13,15] whereas, in another study, no stabilizing effect was observed by adding SiO_2 into CDP in either dry or

[a] *Department of Mechanical Engineering, University of South Carolina, Columbia, South Carolina, 29208, USA. E-mail: huang46@cec.sc.edu*
[b] *Engineering Directorate, Lawrence Livermore National Laboratory, Livermore, CA, 94550, USA*

† Electronic supplementary information (ESI) available. See DOI: https://doi.org/10.1039/d4ya00606b

humid environments.[19] It has been reported that adding ZrO_2 into CDP in a molar ratio of CDP : ZrO_2 = 2 : 1 improved the fuel cell performance at 275 °C and p_{H_2O} = 0.12 atm.[20]

Despite the prior efforts to stabilize CDP at higher temperatures or at lower p_{H_2O}, none of them have been practically demonstrated. Searching for solutions/materials to stabilize the CDP phase and conductivity for practical applications is still in high demand. Here in this work, we report on the feasibility of using hydrophilic SnO_2 as a stabilizer for conductivity.[21–23] A total of seven compositions of $(1 - x)$CDP/$x$$SnO_2$ (x = 0 ≤ x ≤ 40 wt%) were prepared and characterized using X-ray diffraction, field emission scanning electron microscopy, energy dispersive X-ray spectroscopy, and Raman spectroscopy, followed by electrochemical impedance spectroscopy (EIS) analysis on CDP–SnO_2 conductivity at 250 °C over a broad range of p_{H_2O}. The CDP–SnO_2 conductivity was particularly evaluated as a function of time at low p_{H_2O} = 0.10 atm, at which pure CDP is known to be unstable. To understand the electrochemical behaviors and degradation mechanisms, post-tested samples were further analyzed by XRD, SEM, FTIR, and Raman spectroscopy. Subsequently, we performed chronoamperometry at 1 V under low p_{H_2O} conditions to acquire the electrochemical H_2 pumping performance. The results of this study support the use of SnO_2-modified CDP-based membranes for hydrogen separation from various H_2-containing gas mixtures such as the products of water gas shift reaction as well as promoting hydrogenation/dehydrogenation reactions.

2. Experimental section

2.1. Sample preparation

Pure CDP was prepared using the co-precipitation method[24] where cesium carbonate (Cs_2CO_3, Alfa Aesar) and phosphoric acid (H_3PO_4, 85% purity, Sigma Aldrich) were used as a precursor in stoichiometric amounts. Initially, Cs_2CO_3 and H_3PO_4 were dissolved in 100 and 50 mL of methanol, respectively, and stirred in separate beakers for 2 hours to form transparent solutions. The solution of H_3PO_4 was then poured into the Cs_2CO_3 solution and stirred together for 5 hours to initiate the reaction $2H_3PO_4 + Cs_2CO_3 \rightarrow 2CsH_2PO_4\downarrow + H_2O + CO_2\uparrow$. Since the formed CDP is insoluble in methanol, it precipitates out as a solid. The precipitate was then filtered out and dried at 80 °C in an oven for 20 hours. The dried powder was mixed with methanol and then ball-milled for 6 hours. After drying, the final product was ready for use in characterization and testing. To prepare the composite of CDP and SnO_2, we simply mixed commercially available SnO_2 powder (Fisher Scientific, mean size 2.71 μm) in the desired ratio as listed in Table 1 with the as-synthesized CDP in an agate mortar for 1 hour.

2.2. X-ray diffraction (XRD)

The phase compositions in the powder form of the pre- and post-tested electrolytes were examined with an X-ray diffractometer (Rigaku MiniFlex II) equipped with Cu Kα radiation (λ = 1.5418 Å) over a 2θ = 15–75° range with a step size of 0.02° and a scanning rate of 2° min^{-1}.[25]

Table 1 Compositions of CDP/SnO_2 composite electrolyte in weight percent and molar ratio

Composite	Symbol	Weight% of SnO_2	Molar ratio (CDP : SnO_2)
Pure CDP	CDP	0	1 : 0
95CDP : 05SnO_2	CS-5	5	12 : 1
90CDP : 10SnO_2	CS-10	10	6 : 1
86CDP : 14SnO_2	CS-14	14	4 : 1
82CDP : 18SnO_2	CS-18	18	3 : 1
75CDP : 25SnO_2	CS-25	25	2 : 1
60CDP : 40SnO_2	CS-40	40	1 : 1

2.3. Field emission scanning electron microscopy (FESEM) and energy dispersive X-ray spectroscopy (EDX)

Microstructures of fresh and post-tested composite electrolytes were characterized by a field emission scanning electron microscope (Zeiss FESEM with EDX) and elemental mapping was studied by energy-disperse X-ray spectroscopy (EDX) to analyze chemical composition.[26]

2.4. Raman spectroscopy

Raman spectroscopy was conducted using Horiba Jobin-Yvon LabRAM HR800 with a 532 nm excitation laser to investigate the vibrational properties of pure and composite pre- and post-test electrolyte samples.[27]

2.5. Electrical conductivity measurements

For the conductivity measurements, the symmetrical cell was constructed by sandwiching a uniaxially co-pressing CDP/SnO_2 pellet with two identical carbon paper electrodes (Toray Carbon Paper 060 Value Pack, Wet Proofed, Fuel Cell Stores) at 300 MPa for 20 minutes. The area of each electrolyte was 3.14 cm^2 (diameter = 20 mm) and thickness was maintained between 1.38 and 1.42 mm. Silver mesh and copper foam were used as current collectors. The experimental setup is illustrated in Fig. S1 (ESI†) and the actual parts used are shown in Fig. S2 (ESI†). EIS spectra were then gathered using a Solartron 1260/1287 electrochemical station within a frequency range of 10^6–1 Hz and an AC signal amplitude of 10 mV under open-circuit voltage (OCV) conditions. The highest-frequency intersection of the collected spectra with the real axis is the bulk resistance of the sample, from which the ionic conductivity was calculated. The experimental conditions include a constant temperature of 250 °C and a time of 12 hours in which p_{H_2O} started from 0.30 atm and decreased by 0.05 atm each time up to p_{H_2O} = 0.10 atm. The H_2O partial pressure was controlled by a water bubbler at a specific temperature (see Table S1, ESI†), through which steam was provided using pure H_2 as a carrier gas. To avoid steam condensation, all gas lines were covered with heating tapes at 100 °C.

2.6. Electrochemical pumping performance evaluation

For the electrochemical hydrogen separation, the membrane electrode assemblies (MEAs) were prepared by a co-pressing method at 300 MPa for 20 minutes, which uses Toray Carbon

Paper 060 Value Pack, Wet Proofed (Fuel Cell stores) as a support; Pt/C was 10% platinum on Vulcan 72 (Fuel Cell stores) as a catalyst, and naphthalene (Sigma Aldrich) in the electrode to make the electrode porous. The symmetrical MEA composition is as follows:

Carbon paper|CDP/SnO_2 + Pt/C + naphthalene|CDP/SnO_2|CDP/SnO_2 + Pt/C + naphthalene|carbon paper. Roughly, 1 gram of the electrolyte and 0.1 gram of the electrode on each side were used in all MEAs to maintain a fixed thickness of 1.62 mm and active area of 3.14 cm^2 (diameter = 20 mm). Silver mesh and copper foam were used as current collectors.

The experimental setup for H_2 pump performance testing is shown in Fig. S3 (ESI†). Although we used the same cell fixture as the conductivity measurement with MEA as mentioned above, the gas supplies are different. In this case, one side of the electrolyte membrane was fed with 5%H_2–N_2 as the H_2 source and another side of the electrolyte membrane was supplied with pure Ar to sweep out H_2. The composition of H_2 + Ar was analyzed by online gas chromatography (Agilent MicroGC 490) for H_2 content, from which the H_2 rate, was derived. To ensure electrolyte stability, both 5%H_2–N_2 and pure Ar were humidified to p_{H_2O} = 0.10 atm levels through a water bubbler set at a specific temperature (47 °C). The constant DC voltage (1 V) was provided by a Solartron 1260/1287 electrochemical workstation. The rate of H_2 as a performance indicator was evaluated as a function of time at 250 °C and p_{H_2O} = 0.10 atm for pure CDP and CS-18.

3. Results and discussion

3.1. Phase composition of CDP/SnO_2 composites

The two-phase nature of CDP and SnO_2 was confirmed by XRD patterns as shown in Fig. 1(a). No extra impurity in the composite was observed. Two-phase Rietveld refinement (details for refined parameters are attached in Table S2, ESI†)[28] was also performed to confirm the mixture of CDP and SnO_2. For this analysis, we considered *P*21/*m* (11) and *P*42/*mnm* (136) space groups for CDP and SnO_2, respectively, and the refined pattern is shown in Fig. 1(b).

3.2. SEM/EDX results

The cross-sectional view of a symmetrical cell consisting of a CDP/SnO_2 electrolyte and porous carbon paper-supported electrode is shown in Fig. 2(a). The bonding between the CDP/SnO_2 composite electrolyte and the electrode is reasonably good, showing no physical cracks or gaps between the two. In addition, Fig. 2(b) and (c) show that the CDP/SnO_2 electrolyte layer is dense in microstructure and uniform in elemental distribution. Fig. 2(d) further indicates the strong presence of Cs, Sn, and P in the composite membrane without other elements.

3.3. Raman spectra

Raman spectroscopy is a powerful technique to detect lattice vibrations in chemical bonds.[29–31] To exploit this technique, we studied all the compositions; the results are shown in Fig. 3, in which the black and grey arrows indicate the Raman shifts for CDP and SnO_2, respectively. All the shifts seen in pure and composite CDP and SnO_2 match well with those reported in the literature; no shifts other than those for CDP and SnO_2 were observed, which agrees with the XRD results.

The specification and assignment of each Raman shift in CDP and SnO_2 are listed in Table 2.[32–34] In the case of CDP, the wavenumber from 300 to 1250 cm^{-1} is mostly related to the lattice vibration of O–P–O and P–O vibrations, whereas higher wavenumber lattice vibrations are dominated by O–H–O and O–H lattice vibrations. There are three types of O–H vibration in CDP: out-of-plan, in-plane, and stretching vibrations. Note that these lattice vibrational shifts may be affected during the test, which can be detected in post-test samples.

For the case of SnO_2 vibrations, the most intense peak belongs to Sn–O symmetric vibration at 631 cm^{-1} and the intensity of this shift aligns linearly with SnO_2 addition in the CDP matrix, see the enlarged view in the inset of Fig. 3. Higher SnO_2 content leads to higher Raman intensity whereas lower intensity in the case of CS-5 and no SnO_2 shift in pure CDP. This indicates that, even with mechanical mixing, SnO_2 particles were properly incorporated into the CDP matrix forming a well-dispersed composite. Interestingly, some of the new shifts

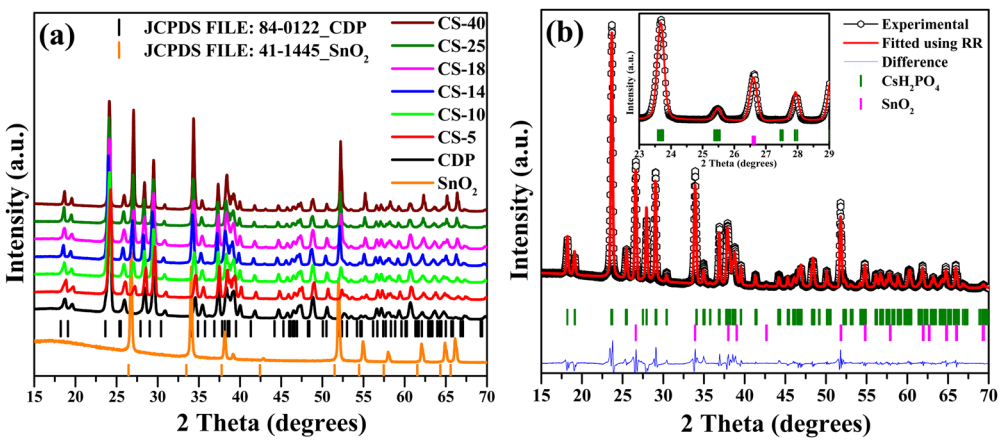

Fig. 1 (a) X-ray diffraction patterns of pure CDP and composite CDP/SnO_2 electrolyte. (b) Rietveld refinement patterns of CS-25 (75CDP : 25SnO_2).

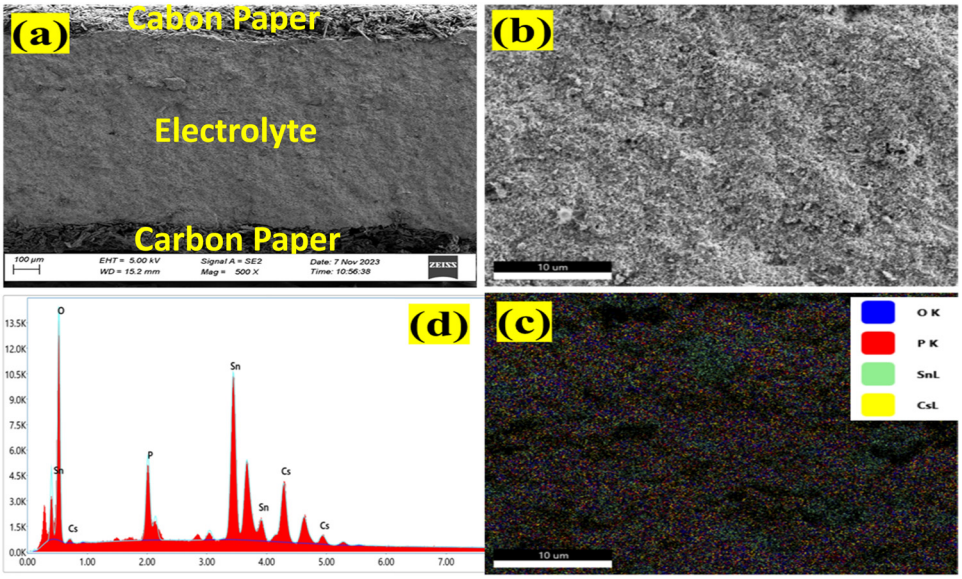

Fig. 2 (a) The cross-sectional view of CDP/SnO_2 sandwiched between carbon paper. (b) and (c) EDX of the CDP/SnO_2 composite electrolyte. (d) The elemental mapping of the CDP/SnO_2 composite electrolyte.

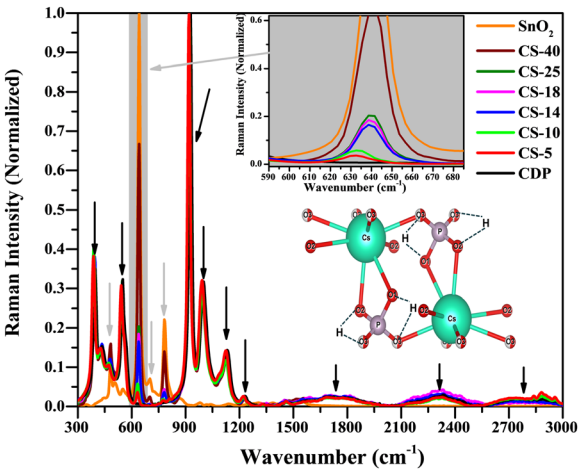

Fig. 3 Raman spectra of the CDP/SnO_2 composite electrolyte; the black arrow indicates shifts corresponding to CDP and the grey arrow indicates shifts related to SnO_2. The representative crystal structure is extracted from VESTA software.

Table 2 Assignment and description of CDP and SnO_2 Raman shifts

Cesium dihydrogen phosphate (CsH_2PO_4) (black arrow ↓ in figure)		
Wavenumber (cm^{-1})	Assignment	Description
389, 471, 561	A_g	(OPO) skeleton bending vibrations
428, 550	B_g	(OPO) skeleton bending vibrations
921, 1000, 1130, 1230	A_g	(PO) skeleton stretching vibrations
1700	A_g	Out-of-plane OH vibrations
2332	A_g	In-plane OH vibrations
2750	A_g	(OH) stretching vibrations
Tin oxide (SnO_2) (grey arrow ↓ in figure)		
Wavenumber (cm^{-1})	Assignment	Description
473	E_g	Vibration of oxygen
631	A_g	Symmetric Sn–O stretching
769	B_{2g}	Asymmetric Sn–O stretching
510, 550, 700	New	Presence of nano-size SnO_2 particles

are observed in SnO_2, implying the presence of nano-SnO_2 particles, see Table 2.

3.4. EIS analysis

The evolution of ionic conductivity of pure CDP as a function of steam content at 250 °C is shown in Fig. 4(a). Up to 260 °C, CDP remains in the superionic phase and does not undergo phase decomposition.[14] At a high steam content of 30%, CDP exhibits a stable conductivity of 1.5×10^{-2} S cm^{-1} for 12 hours. At a further decrease in steam content to 20%, only a small decrease is observed. However, a significant decrease in conductivity is seen at ≤15% steam by approximately one order of magnitude. These results suggest that at least 20% steam is needed to ensure stable conductivity. A conductivity degradation mechanism for CDP under low steam content is dehydration, *i.e.* the material loses its ability to withhold H_2O that is essential to conduct protons.

To minimize the steam dependence of CDP's conductivity, we selected SnO_2 as an additive to CDP; the former is known as a wide-bandgap super-hydrophilic material,[21] and its presence is expected to enhance the water-holding ability within CDP. The conductivity results of different CDP/SnO_2 compositions measured at 250 °C and 10% H_2O are depicted in Fig. 4(b). A comparison with Fig. 4(a) indicates that CDP/SnO_2 composite electrolytes are more stable than pure CDP but with a lowered ionic conductivity to the magnitude of 10^{-3} S cm^{-1}. Taking the 7th-hour data in Fig. 4(b) for comparison purposes, Fig. 4(c) shows a peak conductivity at CS-18 composition. This is clearly

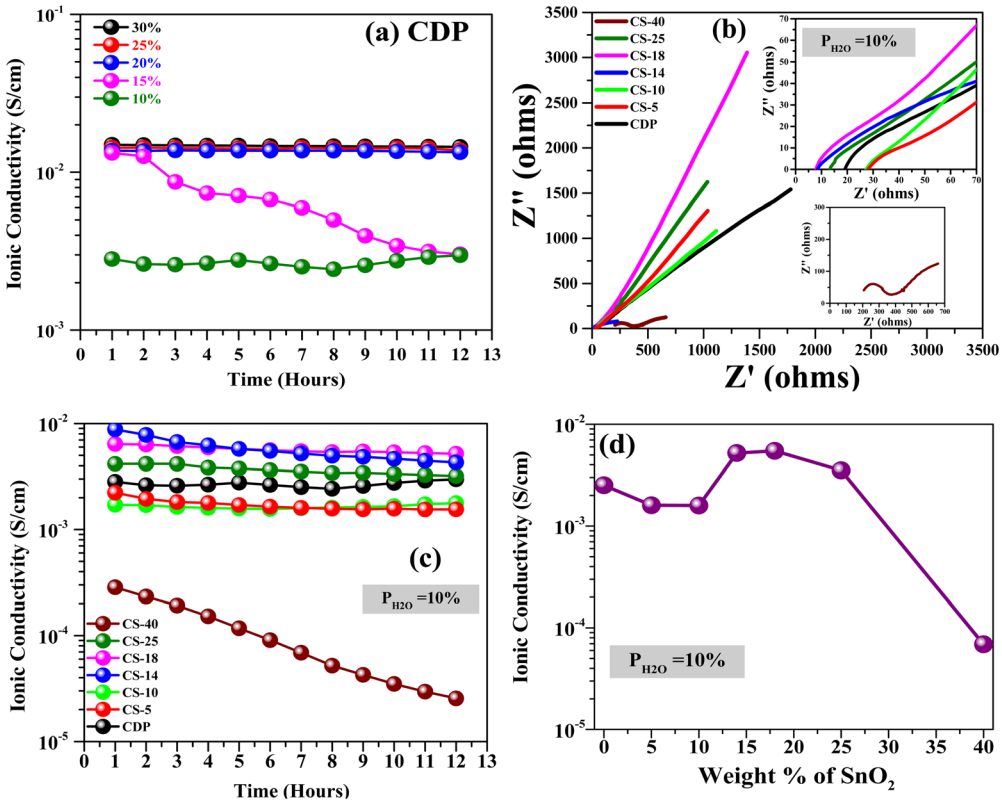

Fig. 4 (a) Time-dependent conductivity of pure CDP electrolyte at 250 °C in wet H_2 atmosphere at a 30 mL min^{-1} flow rate on both sides and different water partial pressure. (b) Time-dependent EIS of the composite CDP/SnO_2 electrolyte at 250 °C in a wet H_2 atmosphere with 30 mL min^{-1} flow rate on both sides and water partial pressure/p_{H_2O} = 10%. (c) Time-dependent conductivity of the composite CDP/SnO_2 electrolyte at 250 °C in a wet H_2 atmosphere with 30 mL min^{-1} flow rate on both sides and water partial pressure/p_{H_2O} = 10%. (d) Variation in the conductivity (each at the 7th hour) of the CDP/SnO_2 composite electrolyte with respect to SnO_2 addition.

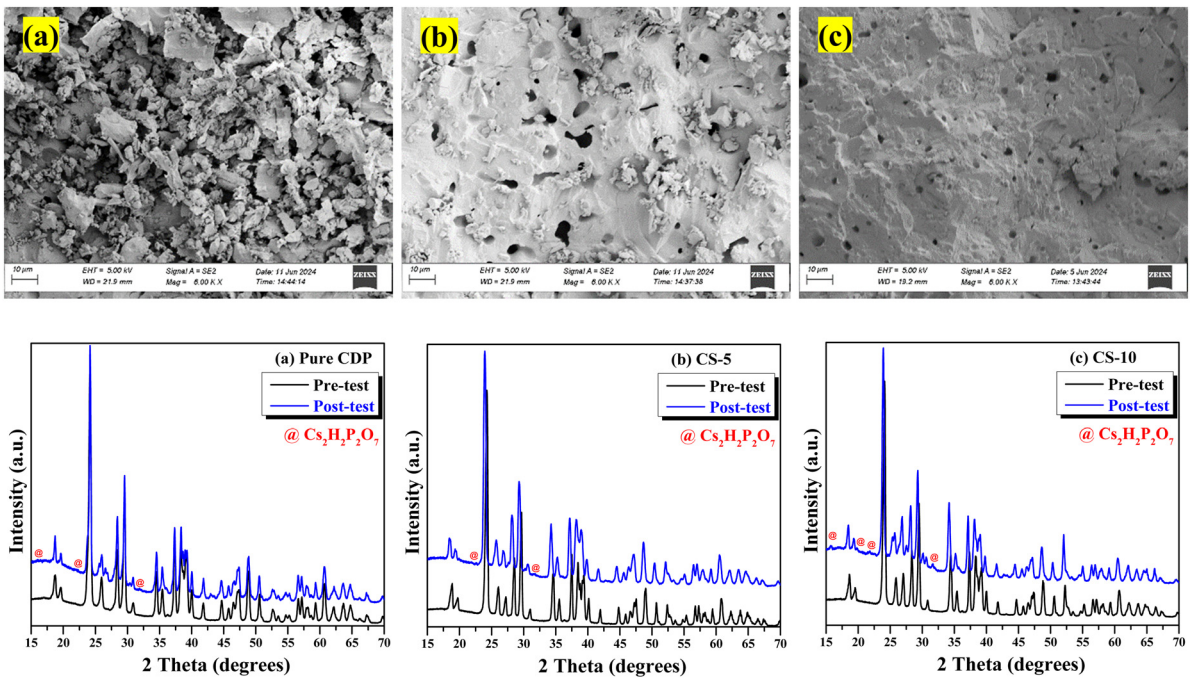

Fig. 5 Pre- and post-test FESEM (cross-sectional) and XRD data; (a) CDP, (b) CS-5, (c) CS-10.

the net result of the retained H_2O and blocked proton conduction in CDP by the presence of SnO_2.

3.4.1. Lower SnO_2 composite electrolytes. Fig. 4(c) indicates that CS-5 and CS-10 exhibit a lower conductivity than pure CDP. To understand this abnormal behavior, we performed the post-test FESEM, XRD, FTIR, and Raman measurements on pure CDP, CS-5 and CS-10 samples. The microstructure of the post-tested CDP in 10%H_2O is shown in Fig. 5(a) with a significant amount of porosity. These pores are left behind as H_2O in CDP and are lost from the body. As H_2O is lost, cubic CDP transforms to non-cubic $Cs_2H_2P_2O_7$ with poor proton conduction. XRD patterns of the post-tested CDP in Fig. 5(a) support the above dehydration hypothesis. For CS-5 and CS-10, Fig. 5(b) and (c) of SEM images clearly shows fewer pores, suggesting that SnO_2 addition helps in retaining the moisture content. The residual pores observed are likely derived from the dehydration of CDP particles. The corresponding XRD patterns of the tested CS-5 and CS-10 in Fig. 5(b) and (c) still show the decomposition products $Cs_2H_2P_2O_7$, implying that low SnO_2 addition cannot stabilize the CDP electrolyte. The major cause for the low conductivity of CS-5 and CS-10 is the presence of the $Cs_2H_2P_2O_7$ dehydration phase, which does not help in saving H_2O but allows faster dehydration, leading to fast conductivity decay as pure CDP. The p_{H_2O}-dependent study of CS-5 and CS-10 is shown in Fig. S4(a) and (b) (ESI†), which reveals that even higher p_{H_2O} does not stabilize the super-protonic phase with lower SnO_2 loading.

3.4.2. Moderate SnO_2 composite electrolytes. For the moderate compositions, CS-14 and CS-18, Fig. 4(d) indicates the highest protonic conductivity. To understand the underlying reason, FESEM imaging was carried out and the results are shown in Fig. 6(a) and (b). It is evident that the number and size of pores are significantly less than CS-5 and CS-10. More importantly, no initial dehydration phase of $Cs_2H_2P_2O_7$ is found in the post-test XRD patterns, see Fig. 6(a) and (b) for CS-18 but in CS-14 only one sharp peak is noticed near 22.5 °C, probably due to slight dehydration. The suppressed dehydration of CDP by a moderate amount of SnO_2 confirms our hypothesis that the hydrophilic (capability to hold water) nature of SnO_2 can stabilize CDP even at low p_{H_2O}. To provide evidence of water withholding SnO_2, we performed FTIT on post-tested samples and the results are shown in the later section.

3.4.3. Higher SnO_2 composite electrolytes. At the highest SnO_2 content, CS-25 and CS-40, Fig. 4(d) indicate a decrease in conductivity, particularly for CS-40. Fig. 7(a) and (b) shows SEM images depicting the densest microstructure among all for CDP/SnO_2 compositions; no pores were found. However, the XRD pattern shown in Fig. 7(a) and (b) indicates significant dehydration of CDP into $Cs_2H_2P_2O_7$ and peaks of the secondary SnP_2O_7 phase probably due to higher SnO_2 content. Also noted is that the peak intensity of SnO_2 surpasses that of CDP. Thus, a major cause for the loss of conductivity at higher SnO_2 content could be the formation of secondary phases of SnP_2O_7, giving rise to a "conductor–insulator" type percolation effect.[16] The p_{H_2O}-dependent

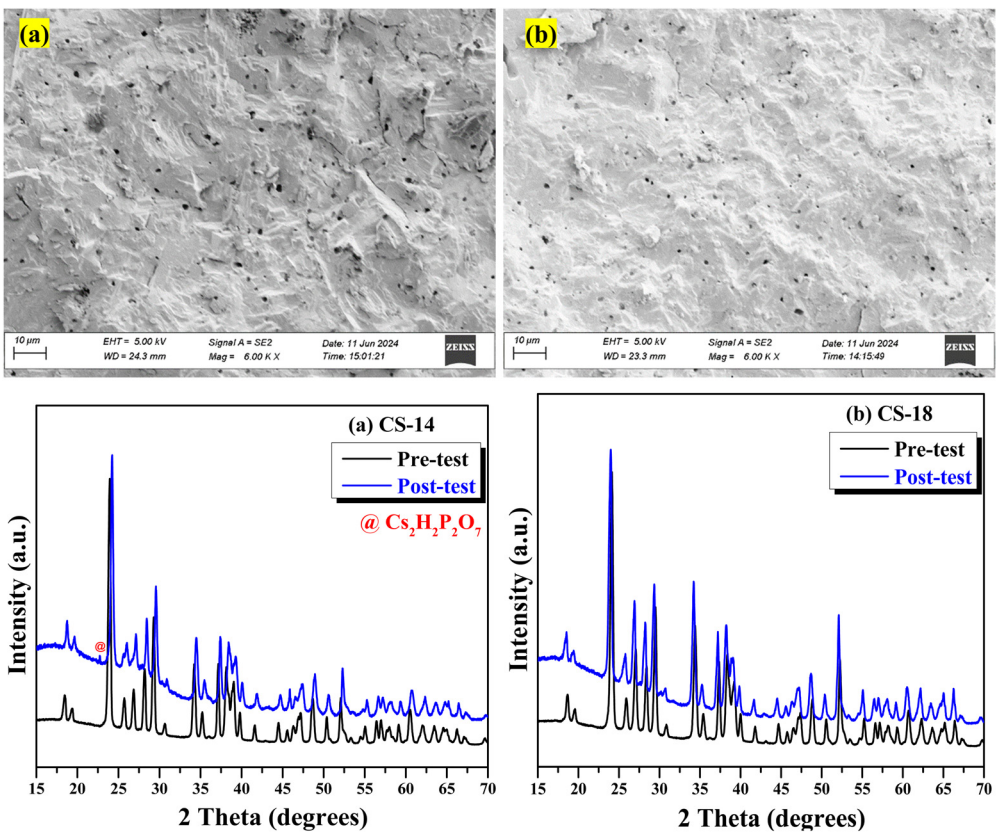

Fig. 6 Pre- and post-test FESEM (cross-sectional) and XRD data; (a) CS-14, (b) CS-18.

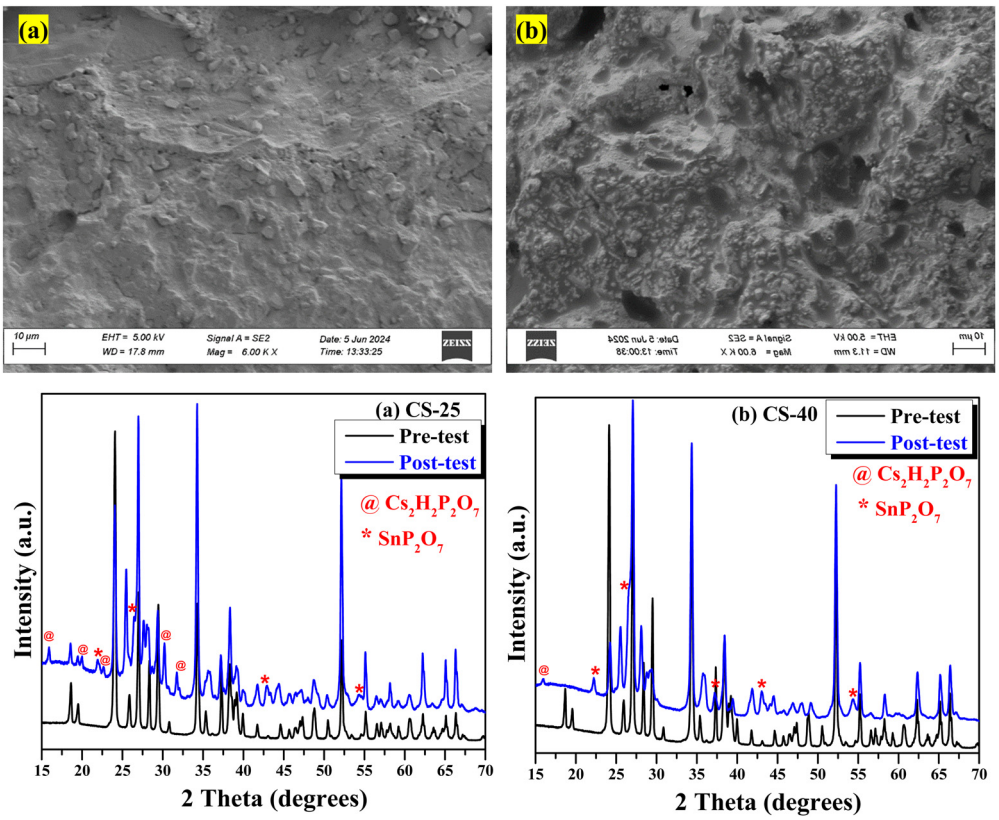

Fig. 7 Pre- and post-test FESEM images (cross-sectional) and XRD patterns; (a) CS-25, (b) CS-40.

study of CS-25 and CS-40 is shown in Fig. S4(c) and (d) (ESI†), which indicates that at higher p_{H_2O} (0.25–0.30 atm) can stabilize the CS-25 and CS-40 electrolytes but a decrease in the conductivity is observed for lower p_{H_2O}. Raman spectra (Fig. S5(a)–(g), ESI†) confirmed the XRD findings. Notably, the Raman intensity of (OH) vibrations does not change much in the CS-40 sample (Fig. S5(g), ESI†), which signals lower proton conduction and vanishing of H^+ due to the formation of SnP_2O_7.

Overall, we have observed that SnO_2 helps in stabilizing the CDP electrolyte at lower p_{H_2O}, and all compositions show stable conductivity greater than 10^{-3} S cm^{-1} at 250 °C and 10%H_2O, except for CS-40. Among all the composites, for the CDP/SnO_2 electrolytes discussed above, moderate SnO_2 addition to CDP shows the best performance. Therefore, in the next section, we will further discuss the conductivities of CS-14 and CS-18 samples at 250 °C as a function of p_{H_2O}.

3.5. Conductivities of CS-14 and CS-18 *versus* p_{H_2O}

Fig. 8(a) and (b) shows the measured conductivity evolution with time at 250 °C under different H_2O contents. The conductivities of both the moderate SnO_2 samples are higher at higher H_2O, but in general, become lower and less stable under lower H_2O. A close comparison of the conductivity values between the two samples in Fig. 8(c) at the 7th-hour marker shows a similar level at <20% H_2O but higher than that of pure CDP. At higher H_2O content, the differences among CS-14, CS-18 and pure CDP becomes indiscernible. Therefore, for fuel cell and H_2 pump applications with low H_2O feedstock, CS-18 is a better choice than pure CDP.

3.6. FTIR evidence of H_2O and SnO_2 interaction

To understand the beneficial effect of SnO_2 on retaining the stability of CDP, FTIR was carried out on pre- and post-test samples to probe the H and OH-bonding information; the results are shown in Fig. 9(a)–(h). For pure CDP, the vibrations related to the P–O are seen in the wavenumber range from 700–1250 cm^{-1} (highlighted by grey color), whereas long and short O–H vibrations are observed above 1500 cm^{-1} as indicated by the blue color arrow in all figures. For CDP/SnO_2 samples, the FTIR spectra of the pre-test samples matched well with the pure CDP, and no new functional group was found. However, for the post-test samples, a new peak was observed between 3000 to 3500 cm^{-1}. Based on the literature data, this peak can be assigned to water molecules bonded with SnO_2 particles, generally denoted as Sn–OH.[35] Interestingly, the sample with moderate SnO_2 loading (CS-14 and CS-18) exhibits the broadest peak compared to other compositions, implying the strongest Sn–OH interaction. The finding of the Sn–OH peak supports the assumption that hydrophilic SnO_2 helps retain local water to stabilize CPD even at lower p_{H_2O}.

3.7. Electrochemical hydrogen pump performance

The CS-18 composition was selected as the electrolyte for our H_2 pump testing as it showed the best stability compared to all

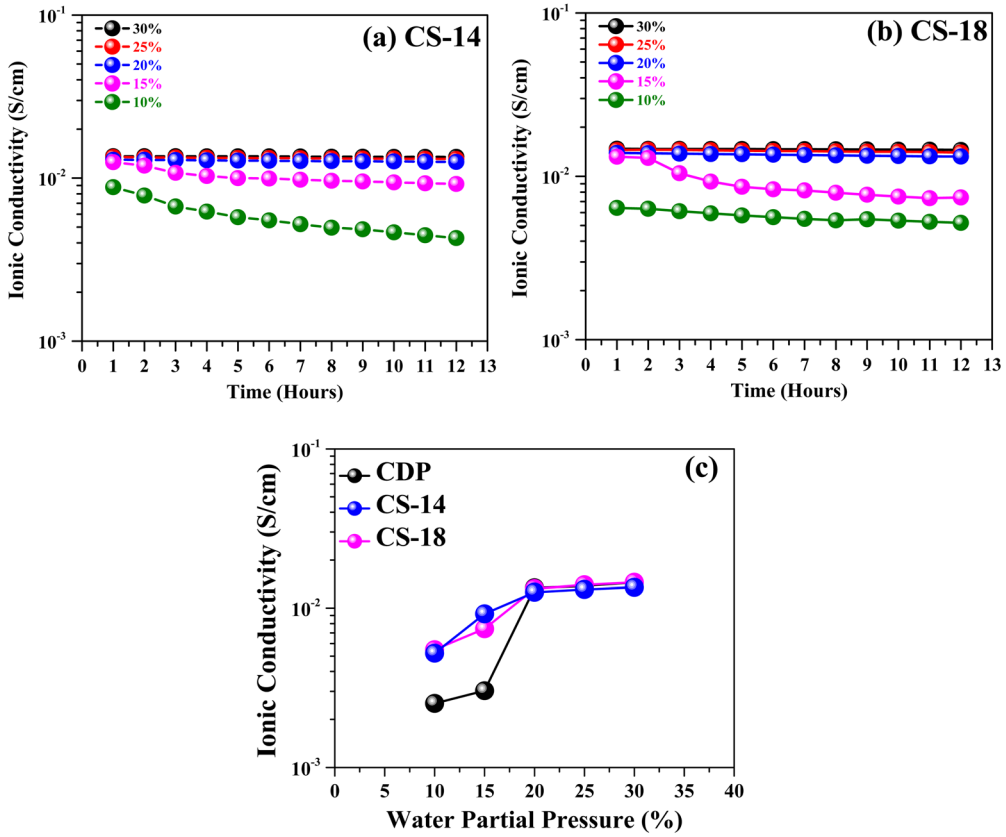

Fig. 8 Time-dependent conductivity of composite electrolytes at 250 °C in wet H_2 atmosphere with 30 mL min^{-1} flow rate on both sides at different water partial pressures: (a) CS-14 and (b) CS-18. (c) Comparative conductivities of CDP, CS-14, and CS-18 at different partial pressures.

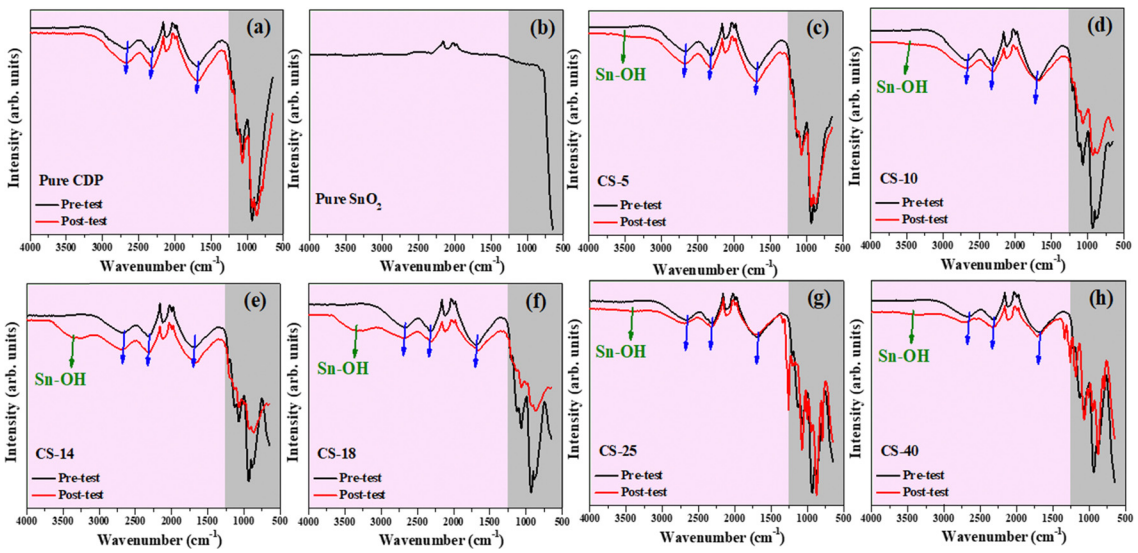

Fig. 9 (a)–(h) FTIR spectra for pure and composite CDP/SnO_2 electrolytes.

the other electrolyte compositions. To avoid the splitting of water that can occur above 1.23 V (ideally) due to the presence of external steam, we performed chronoamperometry at 1 volt with p_{H_2O} = 0.10 atm to examine electrochemical H_2 pumping performance at 250 °C for CS-18 and CDP electrolytes. Fig. 10(a) and (b) show variations in current densities and H_2 flux with time. For the CS-18 electrolyte, the pump current density and H_2 flux exhibit a slight decline before becoming flattened, while

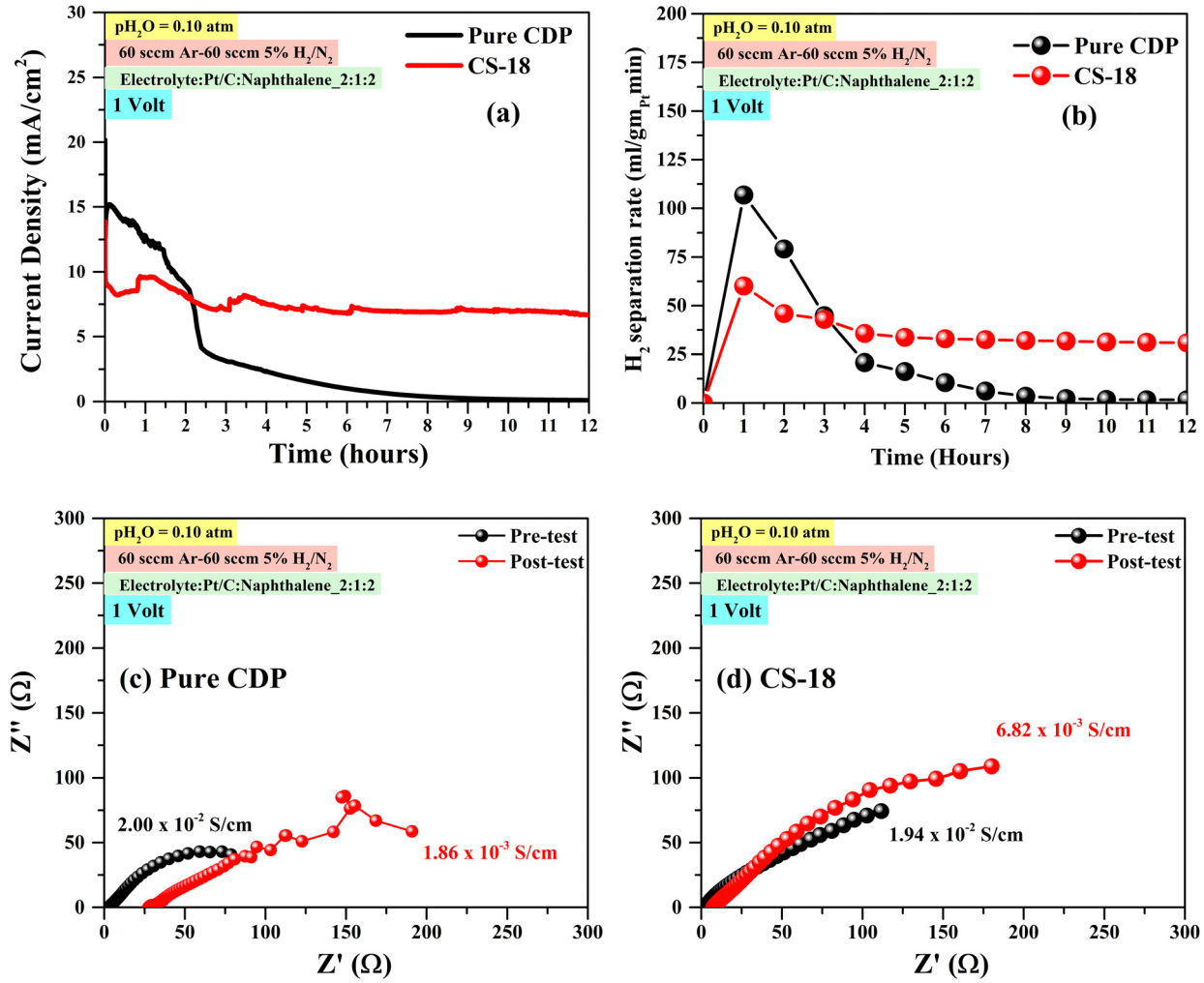

Fig. 10 (a) Chronoamperometry at 1 volt, 250 °C and p_{H_2O} = 0.10 for CS-18 and CDP membrane. (b) The rate of H_2 pumped at 1 volt. (c) and (d) EIS spectra of the pre- and post-test samples.

for the CDP electrolyte, the pump current density and H_2 flux show a continuous decrease with time. Fig. 10(c) and (d) of EIS spectra suggest that the current/flux decline could be due to the decrease in the ionic conductivity of the electrolyte and electrode resistance for initial hours. Overall, we have demonstrated stable electrochemical H_2 pumping performance using CDP/SnO_2 electrolytes at lower p_{H_2O}.

4. Conclusions

In this study, a range of hydrophilic SnO_2 mass was added into CDP to improve the conductivity stability of the latter. The conductivity results show that 18 wt% SnO_2 is the optimal content to achieve balanced conductivity and stability in CDP over a wider range of p_{H_2O}. At too low SnO_2 content, it is insufficient to suppress the dehydration of CDP at lower p_{H_2O}, thus causing conductivity decay. At too high SnO_2 content, on the other hand, it blocks the CDP protonic pathway by the formation of a secondary phase, thus significantly lowering the protonic conductivity. The signature of Sn–OH as an indicator of water retaining ability of SnO_2 is confirmed by FTIR spectra in the post-tested SnO_2-added CDPs. Overall, 18 wt% SnO_2-added CDP represents a stability-conductivity balanced proton conductor that can potentially find applications in fuel cells, electrolyzers and H_2 pumps. Subsequently, stable electrochemical H_2 pumping performance is demonstrated with 18 wt% SnO_2-added CDP electrolyte and Pt/C electrode at p_{H_2O} = 0.10 atm. Overall, 18 wt% SnO_2–CDP is the best composition with stable conductivity under reduced H_2O conditions and 18 wt% SnO_2–CDP electrolyte with Pt/C electrode as the best membrane electrode assembly (MEA) for electrochemical H_2 pumping for lower water partial pressure applications.

Data availability

The data supporting this article are included as part of the ESI.†

Conflicts of interest

There are no conflicts to declare.

Acknowledgements

We thank the U.S. Department of Energy, Basic Energy Science division for the financial support of the work through award DE-SC0023376. This work was supported by Lawrence Livermore National Laboratory under the auspices of the U.S. Department of Energy under Contract DE-AC52-07NA27344. The LLNL information management release number is LLNL-JRNL-866536.

References

1 S. M. Haile, D. A. Boysen, C. R. I. Chisholm and R. B. Merle, Solid acids as fuel cell electrolytes, *Nature*, 2001, **410**(6831), 910–913.
2 D. A. Boysen, T. Uda, C. R. I. Chisholm and S. M. Haile, High-Performance Solid Acid Fuel Cells Through Humidity Stabilization, *Science*, 2004, **303**(5654), 68–70.
3 S. M. Haile, C. R. I. Chisholm, K. Sasaki, D. A. Boysen and T. Uda, Solid acid proton conductors: from laboratory curiosities to fuel cell electrolytes, *Faraday Discuss.*, 2006, **134**(0), 17–39.
4 A. Goñi-Urtiaga, D. Presvytes and K. Scott, Solid acids as electrolyte materials for proton exchange membrane (PEM) electrolysis: Review, *Int. J. Hydrogen Energy*, 2012, **37**(4), 3358–3372.
5 A. V. Belushkin, I. Natkaniec, N. M. Pakida, L. A. Shuvalov and J. Wasicki, Neutron scattering studies of vibrational spectra and structural transformations in the superionic conductors $CsHSO_4$ and $CsHSeO_4$, *J. Phys. C: Solid State Phys.*, 1987, **20**(5), 671.
6 P. Žguns, K. Klyukin, L. S. Wang, G. Xiong, J. Li and S. M. Haile, *et al.*, Uncovering fast solid-acid proton conductors based on dynamics of polyanion groups and proton bonding strength, *Energy Environ. Sci.*, 2024, **17**(15), 5730–5742.
7 T. Anfimova, A. H. Jensen, E. Christensen, J. O. Jensen, N. J. Bjerrum and Q. Li, $CsH_2PO_4/NdPO_4$ Composites as Proton Conducting Electrolytes for Intermediate Temperature Fuel Cells, *J. Electrochem. Soc.*, 2015, **162**(4), F436.
8 V. G. Ponomareva and E. S. Shutova, High-temperature behavior of CsH_2PO_4 and CsH_2PO_4–SiO_2 composites, *Solid State Ionics*, 2007, **178**(7), 729–734.
9 E. Ortiz, R. A. Vargas and B. E. Mellander, On the high-temperature phase transitions of CsH_2PO_4: A polymorphic transition? A transition to a superprotonic conducting phase?, *J. Chem. Phys.*, 1999, **110**(10), 4847–4853.
10 D. Veer, P. Kumar, D. Singh, D. Kumar, A. Kumar and R. S. Katiyar, Phase Behavior and Ionic Conduction in the Composite Electrolytes $CsH_2PO_4/SDP{\cdot}2H_2O$, *Russ. J. Inorg. Chem.*, 2021, **66**(14), 2059–2067.
11 N. Fujiwara, H. Nagase, S. Tada and R. Kikuchi, Hydrogen Production by Steam Electrolysis in Solid Acid Electrolysis Cells, *ChemSusChem*, 2021, **14**(1), 417–427.
12 D. Singh, J. Singh, P. Kumar, D. Veer, D. Kumar and R. S. Katiyar, *et al.*, The Influence of TiO2 on the Proton Conduction and Thermal Stability of CsH2PO4 Composite Electrolytes, *S. Afr. J. Chem. Eng.*, 2021, **37**, 227–236.
13 D. Singh, J. Singh, D. Veer, P. Kumar and R. S. Katiyar, Synergistic effect of SiO_2 on proton conduction and thermal behavior for nanocomposite electrolyte CsH_2PO_4 fuel cells, *J. Mater. Sci.: Mater. Electron.*, 2022, **33**(9), 6524–6535.
14 C. E. Botez, I. Martinez, A. Price, H. Martinez and J. H. Leal, Superprotonic CsH_2PO_4 in dry air, *J. Phys. Chem. Solids*, 2019, **129**, 324–328.
15 P. Kumar, D. Veer, D. Singh and S. L. Meena, A parametric study of crystal structure, phase stability, and conductivity of the novel phosphate-based composite electrolyte, *Appl. Phys. A.*, 2024, **130**(4), 249.
16 V. G. Ponomareva and G. V. Lavrova, New type of composite proton electrolytes based on CsH2PO4 synthesized by mechanical activation, *Mater. Today: Proc.*, 2019, **12**, 9–12.
17 J. Kim, D. Jang, J. Choi, J. Maeng, H. H. Shin and T. Park, *et al.*, Pt-Based Electrocatalyst Modified by CsH2PO4/SiP2O7 for Electrochemical Oxidation of NH3 to H2 in Solid Acid Electrolysis Cell, *Catalysts*, 2023, **13**(4), 707.
18 T. Matsui, T. Kukino, R. Kikuchi and K. Eguchi, Intermediate-Temperature Fuel Cell Employing CsH_2PO_4/SiP_2O_7-Based Composite Electrolytes, *J. Electrochem. Soc.*, 2005, **153**(2), A339.
19 J. H. Leal, H. Martinez, I. Martinez, A. D. Price, A. G. Goos and C. E. Botez, Stability of the superprotonic conduction of $(1\text{-}x)CsH_2PO_4/xSiO_2$ $(0 \leq x \leq 0.3)$ composites under dry and humid environments., *Mater. Today Commun.*, 2018, **15**, 11–17.
20 A. H. Jensen, Q. Li, E. Christensen and N. J. Bjerrum, Intermediate Temperature Fuel Cell Using CsH_2PO_4/ZrO_2-Based Composite Electrolytes, *J. Electrochem. Soc.*, 2013, **161**(1), F72.
21 Q. Liu, X. Wu, B. Wang and Q. Liu, Preparation and superhydrophilic properties of TiO_2/SnO_2 composite thin films, *Mater. Res. Bull.*, 2002, **37**(14), 2255–2262.
22 Talinungsang, D. D. Purkayastha and M. G. Krishna, Dopant controlled photoinduced hydrophilicity and photocatalytic activity of SnO_2 thin films, *Appl. Surf. Sci.*, 2018, **447**, 724–731.
23 S. N. Pusawale, P. R. Deshmukh and C. D. Lokhande, Chemical synthesis of nanocrystalline SnO2 thin films for supercapacitor application, *Appl. Surf. Sci.*, 2011, **257**(22), 9498–9502.
24 D. Dang, B. Zhao, D. Chen, S. Yoo, S. Y. Lai and B. Doyle, *et al.*, A durable polyvinyl butyral-CsH2PO4 composite electrolyte for solid acid fuel cells, *J. Power Sources*, 2017, **359**, 1–6.
25 Y. Wen and K. Huang, Predicting the Rate of Degradation Related to Oxygen Electrode Delamination in Solid Oxide-Ion Electrolyzers, *J. Electrochem. Soc.*, 2024, **171**(3), 034510.
26 C. Morey, Q. Tang, S. Sun and K. Huang, A Kinetic Study on H2 Reduction of Fe3O4 for Long-Duration Energy-Storage-Compatible Solid Oxide Iron Air Batteries, *J. Electrochem. Soc.*, 2023, **170**(10), 104504.
27 K. Zhang, S. Sun and K. Huang, Combined carbon capture and catalytic oxidative dehydrogenation of propane to propylene conversion through a plug-flow dual-phase membrane reactor, *Chem. Eng. J.*, 2024, **481**, 148395.

28 H. M. Rietveld, A profile refinement method for nuclear and magnetic structures, *J. Appl. Crystallogr.*, 1969, **2**(2), 65–71.
29 M. Gupta, O. V. Rambadey, S. C. Shirbhate, S. Acharya, A. Sagdeo and P. R. Sagdeo, Probing the Signature of Disordering and Delocalization of Oxygen Vacancies and Anti-site Defects in Doped $LaAlO_3$ Solid Electrolytes, *J. Phys. Chem. C*, 2022, **126**(48), 20251–20262.
30 M. Gupta, O. V. Rambadey and P. R. Sagdeo, Probing the effect of R-cation radii on structural, vibrational, optical, and dielectric properties of rare earth (R = La, Pr, Nd) aluminates, *Ceram. Int.*, 2022, **48**(16), 23072–23080.
31 M. Gupta, O. V. Rambadey, A. Sagdeo and P. R. Sagdeo, Investigating the structural, vibrational, optical, and dielectric properties in Mg-substituted $LaAlO_3$, *J. Mater. Sci.: Mater. Electron.*, 2022, **33**(16), 13352–13366.
32 B. Marchon and A. Novak, Vibrational study of CsH_2PO_4 and CsD_2PO_4 single crystals, *J. Chem. Phys.*, 1983, **78**(5), 2105–2120.
33 K. K. Singha, P. P. Singh, R. Narzary, A. Mondal, M. Gupta and V. G. Sathe, *et al.*, Crystal Structure, Raman Spectroscopy and Optical Property Study of Mg-Doped SnO_2 Compounds for Optoelectronic Devices, *Crystals*, 2023, **13**(6), 932.
34 R. N. Mariammal, K. Ramachandran, B. Renganathan and D. Sastikumar, On the enhancement of ethanol sensing by CuO modified SnO_2 nanoparticles using fiber-optic sensor, *Sens. Actuators, B*, 2012, **169**, 199–207.
35 P. A. Luque, O. Nava, C. A. Soto-Robles, H. E. Garrafa-Galvez, M. E. Martínez-Rosas and M. J. Chinchillas-Chinchillas, *et al.*, SnO_2 nanoparticles synthesized with Citrus aurantifolia and their performance in photocatalysis, *J. Mater. Sci.: Mater. Electron.*, 2020, **31**(19), 16859–16866.